Multifrequency synthesis using two coupled nonlinear oscillator arrays

Antonio Palacios,* Ricardo Carretero-González,† Patrick Longhini, and Norbert Renz
Nonlinear Dynamical Systems Group‡, Department of Mathematics and Statistics, San Diego State University, San Diego, California 92182, USA

Visarath In,§ Andy Kho, Joseph D. Neff, Brian K. Meadows, and Adi R. Bulsara
Space and Naval Warfare Systems Center, Code 2363, 53560 Hull Street, San Diego, California 92152-5001, USA
(Received 27 September 2004; revised manuscript received 12 May 2005; published 18 August 2005)

We illustrate a scheme that exploits the theory of symmetry-breaking bifurcations for generating a spatio-temporal pattern in which one of two interconnected arrays, each with N Van der Pol oscillators, oscillates at N times the frequency of the other. A bifurcation analysis demonstrates that this type of frequency generation cannot be realized without the mutual interaction between the two arrays. It is also demonstrated that the mechanism for generating these frequencies between the two arrays is different from that of a master-slave interaction, a synchronization effect, or that of subharmonic and ultraharmonic solutions generated by forced systems. This kind of frequency generation scheme can find applications in the developed field of nonlinear antenna and radar systems.

DOI: 10.1103/PhysRevE.72.026211 PACS number(s): 05.45.−a

I. INTRODUCTION

Many natural and artificial nonlinear systems are made up of oscillating components or cell units that interact with each other to produce complex spatio-temporal patterns of collective behavior. Examples of such systems include arrays of Josephson junctions [1–3], central pattern generators in biological systems [4–10], arrays of coupled lasers [11,12], communication systems via chaotic oscillators [13,14], competing species in population dynamics [15–17], bubble behavior in fluidization and mixing processes [18], fireflies that emit rhythmic light pulses [19,20], and, in particular, active nonlinear antenna and radar systems [21,22].

In advanced radar and antenna systems, it is desirable to have the oscillator arrays be capable of producing multiple frequencies so that one design can be operated in many bands. This would make the system more adaptable and flexible based on the operational needs that are required in modern systems. In active antenna and radar systems, the combined functions of the resonators, the beamformer and the steering array [22] are composed of coupled nonlinear unit cells, such as Van der Pol oscillators, which dynamically interact with one another to form a phase and amplitude pattern to create the desirable beam characteristics, contrasted to passive linear elements in the traditional antenna and radar designs that act independently and rely on many external components such as phase shifters and steering computers to move and shape the beam.

In recent years, theoretical and experimental evidence has been found that symmetry alone can lead to different patterns of "multifrequency" behavior [4,23–27]. In Ref. [23], for instance, it is shown that a ring of N oscillators possessing $\mathbb{D}_N$ symmetry (symmetry of an N-gon) can induce, under certain conditions, an external oscillator to oscillate at N times the collective frequency of the ring. The actual conditions require that the ring oscillates in a traveling wave pattern and that the cross coupling be directed from the ring to the external oscillator, i.e., a master-slave system. An alternative approach is to use the existing theoretical work [24–26,28–30], which shows (within the context of a coupled cell system) that $\mathbb{Z}_N$ symmetry-breaking Hopf bifurcations can also lead to multifrequency patterns. We remark that this approach is significantly different from that of subharmonic and ultraharmonic motion generated via a forced system as is described by Hale and Gambill [31] and later by Tiwari and Subramanian [32]. In our case, the multifrequency behavior arises from the mutual interaction of two arrays of oscillators. None of the oscillators is forced and, consequently, the arrays are naturally modeled by an autonomous system instead of the nonautonomous system that is described in the same references [31,32].

In previous work [33], we used this second approach to show, experimentally, the existence of multifrequency patterns in an electronic circuit that serves as a model for a network of two arrays of over-damped Duffing oscillators coupled to one another. In this work, we address (within the context of coupled nonlinear oscillators) the fundamental issue of whether the $\mathbb{Z}_N$ multifrequency patterns arise from a master-slave scenario or whether they can be obtained from the mutual interaction between the natural dynamics of each array. From experimental and application points of view, we also consider the issue of feasibility and efficiency in a set of mutually interacting arrays compared to a master-slave interaction. Our aim is to set the groundwork for future experiments and applications using Van der Pol oscillators as the prototype nonlinear system in the analysis, this also being of great relevance to the nonlinear antenna work in Refs. [21,22] since the resonators in those devices are Van der Pol oscillators.

*Electronic address: palacios@euler.sdsu.edu
†URL: http://www-rohan.sdsu.edu/~rcarrete/
‡URL: http://nlds.sdsu.edu
§Electronic address: visarath@spawar.navy.mail

The paper is organized as follows. In Sec. II, we present a self-contained background with ideas and concepts, which should be informative for those readers not familiar with the subject of self-induced oscillations. In Sec. III, we describe the actual network configuration (two coupled arrays of N oscillators per array), then we discuss the existence of multifrequency patterns, followed by a mathematical model supporting such patterns. In Sec. IV we present, in more detail, a bifurcation analysis of the existence, stability and robustness of multifrequency patterns in the network equations. The critical point is the fact that the multifrequency rhythm output achieves optimal response, for realistic operational parameters, in a region where the cross couplings between arrays are of the same order of magnitude. Hence, in realistic situations, these multifrequency rhythms are more efficient in a regime where the arrays mutually interact with one another (in contrast to a master slave type of interaction).

II. BACKGROUND

A. Active antenna systems

Active antenna systems are essentially nonlinear devices that consist of diodes, transistors, and nonlinear oscillators distributed and interconnected in an array configuration. The oscillators are voltage controlled, each tied to simple patch radiators. Each active element is electrically coupled via a strip line—typically to a nearest neighbor but other configurations are also possible—to produce a collective pattern of oscillation, and consequently a radiating beam with a common frequency. By adjusting the varactor bias, the free running frequency of each oscillator can be altered but only over a small range. Original designs tried to suppress the interelement coupling as well as noise. Modern designs, on the contrary, exploit coupling and noise to achieve optimal performance. For instance, it is now known that beam steering can be accomplished by changing the bias on the two oscillators located at the boundaries of the array [21], thus eliminating the need for a mechanically rotating array. Of particular promise is also to exploit the symmetry of a given array to generate radiating beams with multiple frequencies, which can eventually lead to all-in-one antenna devices.

B. Symmetry in systems of differential equations

Symmetry is a geometrical concept that can be defined as the set of transformations that leave an object unchanged. In continuous nonlinear phenomena, the objects are the governing equations, which typically consist of systems of ordinary differential equations (ODEs) or partial differential equations, and the transformations are the changes in the underlying variables that leave the equations unchanged. More formally, consider the following system of ODEs:

$$\frac{dx}{dt} = f(x,\lambda), \tag{1}$$

where $x \in \mathbb{R}^n$, $\lambda \in \mathbb{R}^p$ is a vector of parameters and $f:\mathbb{R}^n \times \mathbb{R}^p \to \mathbb{R}$ is a smooth function. Let γ be a particular time-independent transformation in $\mathbb{R}^n$. Direct substitution of the transformed variable γx into (1) yields $\gamma \dot{x} = f(\gamma x, \lambda)$.

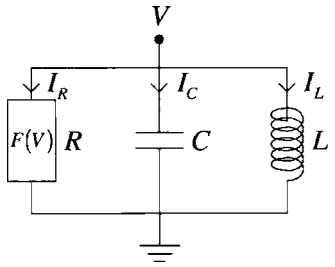

FIG. 1. Circuit realization of a Van der Pol oscillator.

Consequently, for the system of ODEs (1) to remain unchanged, f must commute with γ. In other words, $f(\gamma x) = \gamma f(x)$. In practice, the set of all transformations that commute with f forms a group Γ. We then arrive to the following formal definition.

A system of ODEs such as (1) *is said to have* Γ *symmetry if*

$$f(\gamma x, \lambda) = \gamma f(x, \lambda), \tag{2}$$

for all $x \in \mathbb{R}^n$ *and for all* $\gamma \in \Gamma$.

Equation (2) also implies that f is Γ equivariant. But more importantly, it implies that if x is a solution of (1) then so is $\gamma x(t)$ for all $\gamma \in \Gamma$. As an example, consider the Van der Pol circuit depicted in Fig. 1. I_L and I_C are the currents across the inductor L and capacitor C, respectively. I_R is the current across two resistors R_1 and R_2 located inside the rectangle labeled R in which $F(V) = -V/R_1 + V^3/(3R_2^2)$.

The dynamics of the circuit shown in Fig. 1, after rescaling, is governed by the following second order scalar ODE:

$$\frac{d^2V}{dt^2} - \delta(p - V^2)\frac{dV}{dt} - \omega^2 V = 0, \tag{3}$$

where $\delta = 1/(R_2C)$, $p = R_2/R_1$, $\omega = 1/\sqrt{LC}$. After a change of variables, we can rewrite the model equation (3) as a first order system of the form

$$\frac{dx}{dt} = \delta\left(px - \frac{x^3}{3}\right) + \omega y, \quad \frac{dy}{dt} = -\omega x, \tag{4}$$

where $x(t) = V(t)$. We can then find two transformations that leave this system unchanged, the identity transformation $\gamma_1 = id$, where $\gamma_1(x,y) \mapsto (x,y)$, and a second transformation, which can be described abstractly as $\gamma_2 = -1$, so that $\gamma_2(x,y) \mapsto (-x,-y)$. The identity transformation is always a symmetry of any system, while the second transformation γ_2 corresponds to a reflection through the origin in the phase space $\mathbb{R}^2$. Furthermore, it can be shown that γ_1 and γ_2 are the only transformations that leave (4) unchanged. Together, γ_1 and γ_2 form the group $\mathbb{Z}_2 = \{\gamma_1, \gamma_2\}$ of symmetries of the Van der Pol oscillator (4).

C. Coupled cell systems

A natural mathematical framework for the analysis of arrays of coupled nonlinear oscillators is that of coupled cell system. By a "cell" we mean an individual component or unit that possesses its own dynamical behavior. In what fol-

lows, we assume N identical cells, and consider the internal dynamics of each cell to be governed by a k-dimensional continuous-time system of differential equations of the form

$$\frac{dX_i}{dt} = f(X_i, \lambda), \tag{5}$$

where $X_i=(x_{i1},\ldots,x_{ik}) \in \mathbb{R}^k$ denotes the state variables of cell i and $\lambda=(\lambda_1,\ldots,\lambda_p)$ is a vector of parameters. Observe that f is independent of i because the cells are assumed to be identical. In engineering applications to nonlinear antenna technology, for instance, it is common for the cell dynamics to be described by electrical oscillators such as the Van der Pol oscillator [21,22].

A network of N cells is a collection of identical cells interconnected in some fashion. We model the network by the following system of coupled differential equations:

$$\frac{dX_i}{dt} = f(X_i, \lambda) + \sum_{j \to i} c_{ij} h(X_i, X_j), \tag{6}$$

where h is the coupling function between two cells, the summation is taken over those cells j that are coupled to cell i, and c_{ij} is a matrix of coupling strengths. Additionally, if we let $X=(X_1,\ldots,X_N)$ denote the state variable of the network, then we can write (6) in the simpler form

$$\frac{dX}{dt} = F(X),$$

where the dependence in the parameters λ has been omitted for brevity.

D. Local and global symmetries

Following the work of Dionne *et al.* [34,35], we distinguish *local* symmetries from *global* symmetries as follows. Let $\mathbf{O}(n)$ be the group of orthogonal transformations in R^n. Then $\mathcal{L} \subset \mathbf{O}(k)$ is the group of local or internal symmetries of individual cells if, for all $l \in \mathcal{L}$, we have

$$f(lX_i, \lambda) = lf(X_i, \lambda).$$

While local symmetries are dictated by f, global symmetries are described by the coupling pattern. More precisely, $\mathcal{G} \subset \mathbf{O}(N)$ is the group of global symmetries of the network if, for all $\sigma \in \mathcal{G}$, we have

$$F(\sigma X) = \sigma F(X).$$

III. MODELING

A. Network configuration

We consider a network of oscillators made up of two arrays of Van der Pol oscillators coupled to one another as shown schematically in Fig. 2. Each array contains N identical oscillators, which are each coupled to its two nearest neighbors via diffusive coupling. The internal dynamics of each oscillator cell is governed by (4), thus $\mathbb{Z}_2=\{I_2,-I_2\}$ is the group of local symmetries of each cell, where I_2 is the 2×2 identity matrix. On the other hand, the underlying

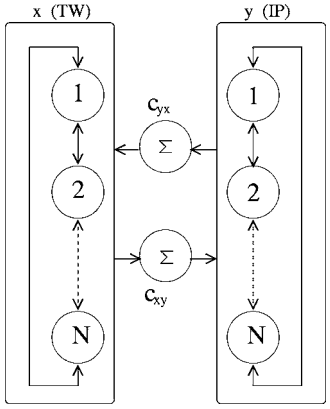

FIG. 2. Schematic diagram of a coupled cell system formed by two arrays of Van der Pol oscillators. Each arrays contains N oscillators, each coupled to its two nearest neighbors.

group of global symmetries of each array is $\mathbb{Z}_N$, i.e., the group of cyclic permutations of N objects. It follows that $\mathbb{Z}_N \times \mathbb{Z}_N$ is the group of global symmetries of the network, including the two interconnected arrays. Every element $\gamma \in \mathbb{Z}_N \times \mathbb{Z}_N$ is composed of a pair of cyclic permutations $\gamma=(\gamma_1,\gamma_2)$, where γ_1 acts on one array and γ_2 acts on the other. Since cyclic and anticyclic permutations are conjugate of each other, the results are essentially the same, except that the traveling waves with cyclic symmetries travel in the opposite direction of those with anticyclic symmetry. Then we only need to consider one group of symmetries. We choose cyclic permutations.

A critical observation is the fact that $\mathbb{Z}_3$ symmetry-breaking Hopf bifurcation leads to a spatio-temporal pattern in which one of the arrays oscillates N times faster than the other [28–30]. Next we present more details of this fact followed by a bifurcation analysis of the emergent pattern.

B. Multifrequency pattern with $\mathbb{Z}_N \times \mathbb{S}^1$ symmetry

To study the collective behavior of the network, we use $X(t)=(X_1(t),\ldots,X_N(t))$ to represent the state of one array and $Y(t)=(Y_1(t),\ldots,Y_N(t))$ to denote the state of the second array. Thus, at any given time t, a spatio-temporal pattern generated by the network can be described by $P(t)=(X(t),Y(t))$. Let us assume that this pattern is a periodic solution of period T with the following characteristics. On one side of the network, for instance, the X array, the oscillators form a traveling wave (TW), i.e., same wave form X_0 shifted (delayed) by a constant time lag $\phi=T/N$, $X_k(t)=X_0[t+(k-1)\phi]$, $k=1,\ldots,N$. On the opposite side, the oscillators are assumed to be in-phase (IP) with identical wave form Y_0, i.e., a synchronous state, $Y_k(t)=Y_0(t)$, $k=1,\ldots,N$. Now assume that $P(t)$ has spatio-temporal symmetry described by the cyclic group $\mathbb{Z}_N$, i.e., the group of cyclic permutations of N objects generated by $(1,2,\ldots,N)\mapsto(N,1,\ldots,N-1)$, and by the group $\mathbb{S}^1$ of temporal shifts. Together, $\mathbb{Z}_N \times \mathbb{S}^1$ acts on $P(t)$ as follows. First, $\mathbb{Z}_N$ cyclically permutes the oscillators of both arrays,

$$\mathbb{Z}_N X_{\mathrm{TW}}(t) = \{X_N[t+(N-1)\phi], X_1(t), \ldots, X_{N-1}[t+(N-2)\phi]\},$$

$$\mathbb{Z}_N Y_{\mathrm{IP}}(t) = \{Y_N(t), Y_1(t), \ldots, Y_{N-1}(t)\}.$$

Then $\mathbb{S}^1$ shifts time by ϕ so that

$$\mathbb{Z}_N \times \mathbb{S}^1 X_{\mathrm{TW}}(t) = \{X_N(t), X_1(t+\phi), \ldots, X_{N-1}[t+(N-1)\phi]\},$$

$$\mathbb{Z}_N \times \mathbb{S}^1 Y_{\mathrm{IP}}(t) = \{Y_N(t+\phi), Y_1(t+\phi), \ldots, Y_{N-1}(t+\phi)\}.$$

Since the oscillators are identical, we get

$$\mathbb{Z}_N \times \mathbb{S}^1 X_{\mathrm{TW}}(t) = X_{\mathrm{TW}}(t),$$

$$\mathbb{Z}_N \times \mathbb{S}^1 Y_{\mathrm{IP}}(t) = Y_{\mathrm{IP}}(t+\phi).$$

It follows that in order for $Y_{\mathrm{IP}}(t)$ to have $\mathbb{Z}_N \times \mathbb{S}^1$ symmetry the in-phase oscillators must oscillate at N times the frequency of the oscillations of the traveling wave. The same conclusion is reached if the roles of the X and Y arrays are interchanged.

C. Model equations

We now provide evidence of the existence of a multifrequency pattern such as $P(t)$. We conduct numerical simulations of a differential equation model for the network shown in Fig. 2, with $N=3$ Van der Pol oscillators per array (results with larger N are also provided). In order to facilitate the bifurcation analysis of the following section, we rewrite the internal dynamics of each Van der Pol oscillator (4) in normal form [21]

$$\dot{z} = (\alpha + \omega i) z - |z|^2 z,$$

where $z \in \mathbb{C}$ is now the state variable and α and ω are parameters. Observe that the $\mathbb{Z}_2$ symmetry of (4) is preserved by the normal form. Then we model the network by the following system of coupled differential equations:

$$\begin{aligned}\dot{x}_j &= (\alpha_x + \omega_x i) x_j - |x_j|^2 x_j + c_x (x_{j-1} + x_{j+1} - 2x_j) \\ &\quad + c_{yx} \sum_{k=1}^{N} |y_k|, \quad j = 1, \ldots, N \bmod(N), \\ \dot{y}_j &= (\alpha_y + \omega_y i) y_j - |y_j|^2 y_j + c_y (y_{j-1} + y_{j+1} - 2y_j) \\ &\quad + c_{xy} \sum_{k=1}^{N} |x_k|, \quad j = 1, \ldots, N \bmod(N), \end{aligned} \tag{7}$$

where $x_j \in \mathbb{C}$ and $y_j \in \mathbb{C}$ describe the state of the jth cell of the X and Y arrays, respectively, c_x and c_y represent the coupling strength within the X and Y arrays, respectively; and c_{xy} and c_{yx} describe the cross-coupling strengths from the X array to the Y array and vice versa, respectively. Figure 3 shows the results of integrating the model equations (7) with $N=3$ and $(c_{xy}, c_{yx}) = (0.12, 0.12)$. The period of the traveling wave is approximately $T \approx 13.272$ s (frequency ≈ 0.0753 Hz). As predicted by theory, the in-phase oscillations of the Y array are three times faster (see power spectra densities in lower panels) than the traveling wave produced by the X array.

A generalization of the existence of similar multifrequency patterns in larger arrays depends upon network connections that can satisfy the necessary conditions for the $\mathbb{Z}_N$ symmetry-breaking Hopf bifurcations, which induce the arrays to oscillate, one in a TW pattern and one in an IP solution. The network configuration shown in Fig. 2 with N odd, in particular, shows similar multifrequency results. We have tested it with up to $N=19$ oscillators. Figure 4 illustrates additional examples. When N is even, however, other coupling schemes need to be considered so that the network can meet the necessary conditions for the Hopf bifurcations. An analysis of the N-even case is deferred for future work.

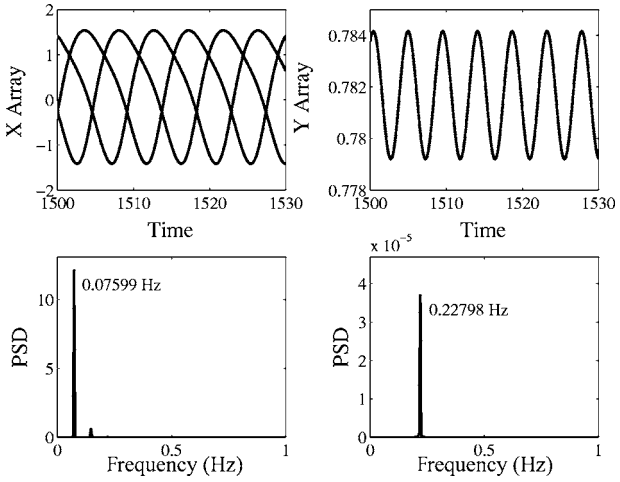

FIG. 3. Multifrequency oscillations found in simulations of network equations (7) with $N=3$. (Left) The X array generates a traveling wave pattern, while the (right) Y array yields an in-phase pattern that oscillates at three times the frequency of the traveling wave. The bottom panels depict the corresponding power spectra density (PSD) where it can be checked that the in-phase pattern has a frequency three times greater than the traveling wave pattern ($0.227\,98 \approx 3 \times 0.075\,99$). Parameters are $\alpha_x = \alpha_y = 1.0$, $\omega_x = \omega_y = 0.5$, $c_x = -0.4$, $c_y = 0.4$, and $c_{xy} = c_{yx} = 0.12$.

IV. BIFURCATION ANALYSIS

We now consider the issue of whether the multifrequency patterns found in the network simulations are simply the result of a master-slave interaction between the X and Y arrays, or whether these patterns can arise from a truly mutual interaction between the two arrays of oscillators. To address this issue, we conduct, next, a numerical bifurcation analysis of the existence and stability of multifrequency solutions of (7) using the continuation package AUTO [36]. We use the stable limit cycle solution found at $(c_{xy}, c_{yx}) = (0.12, 0.12)$, see Fig. 3, which consists of one complete period of the traveling wave and three periods of the in-phase oscillations, as initial condition. We fix $c_{yx} = 0.12$ and then vary c_{xy}. The limit cycle is originally stable but it loses stability as c_{xy} decreases towards $c_{xy} = c_{xy}^{\mathrm{sn1}} = 0.1082$ (SN1), see Fig. 5. To the left of this critical point, the cycle locally disappears in a saddle-node bifurcation. At $c_{xy} = c_{xy}^{\mathrm{sn1}} = 0.1123$, a second turning point SN2 is found but this time the limit cycle is always unstable in the vicinity of SN2. A second pair of saddle-node points, SN3 and SN4, with similar characteristics are also

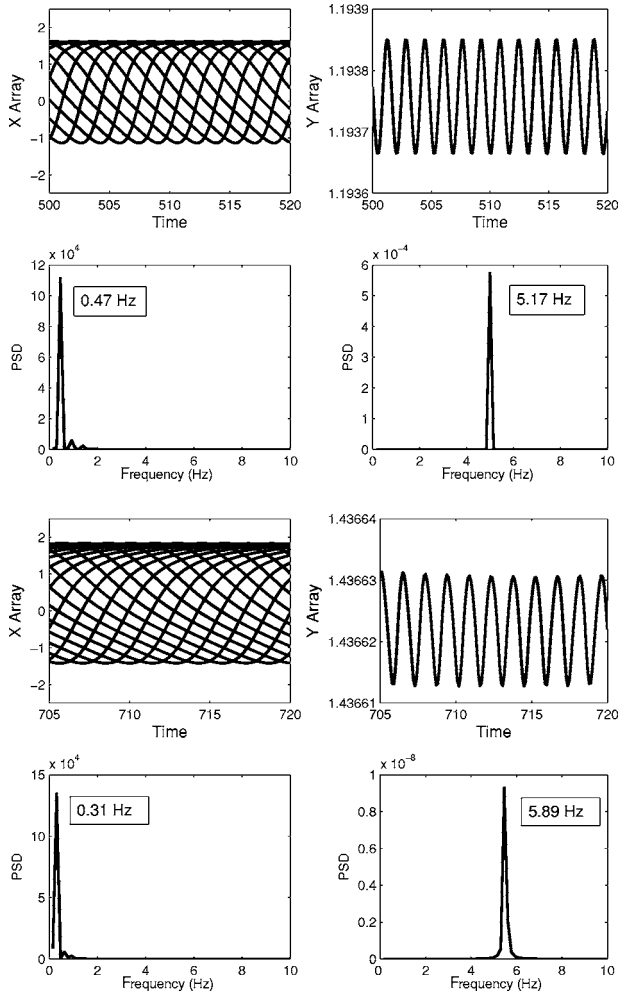

FIG. 4. Additional multifrequency oscillations from simulations of the network equations (7) with (top four panels) $N=11$ oscillators per array and (bottom four panels) $N=19$ oscillators per array. The in-phase pattern Y array has a frequency 11 and 19 times greater, respectively, than that of the traveling wave. Parameters are top panels, $\alpha_x=\alpha_y=1.0$, $\omega_x=\omega_y=0.5$, $c_x=-0.3$, $c_y=0.3$, and $c_{xy}=c_{yx}=0.06$; and bottom panels, $\alpha_x=\alpha_y=1.0$, $\omega_x=\omega_y=0.3$, $c_x=-0.45$, $c_y=0.45$, and $c_{xy}=c_{yx}=0.034$.

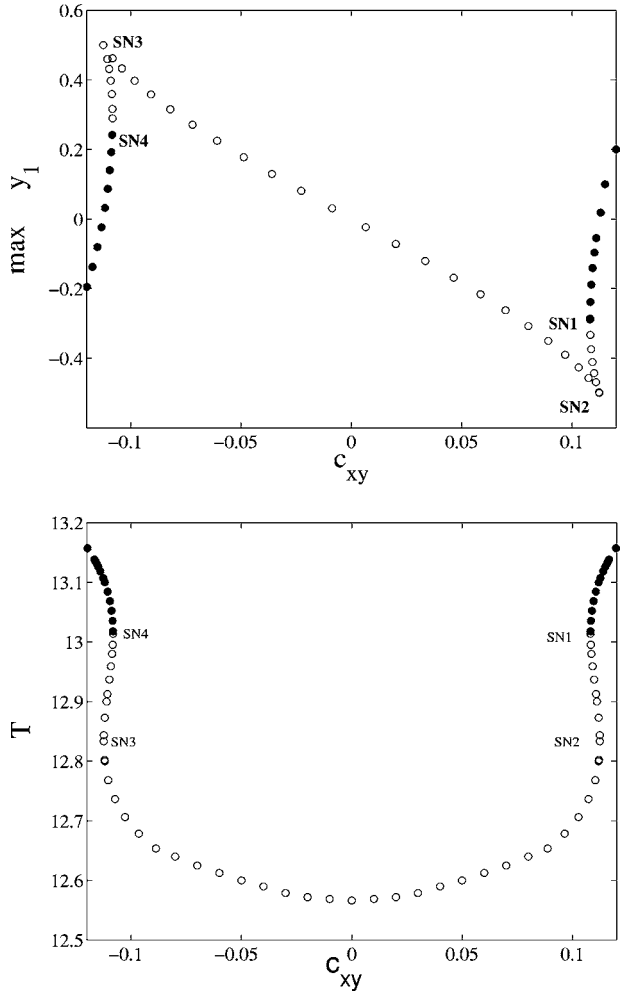

FIG. 5. Bifurcation diagrams for the multifrequency pattern shown in Fig. 3. (Top) Maximum value of first component in the Y array against parameter c_{xy}. (Bottom) Period T of limit cycle solution against c_{xy}. Filled and/or empty circles indicate stable and/or unstable periodic solutions, respectively. All other parameters are the same as in Fig. 3.

found for $c_{xy}<0$ (this is a consequence of the $\mathbb{Z}_2$ symmetry mentioned above). We remark that another consequence of symmetry is the generical occurrence of structurally stable heteroclinic cycles between two or more saddle-node points. As time evolves, a typical trajectory near the cycle stays for increasingly longer periods near each saddle node before it makes a rapid excursion to the next saddle. Geometrically speaking, symmetry tends to create invariant subspaces in phase space through which such cyclic connections can be facilitated by the intersection of stable and unstable manifolds of the saddle nodes. An analysis of these cycles is beyond the scope of the present work. The interested reader, however, is referred to the work by Buono, Golubitsky, and Palacios [4], in which the authors studied the existence and stability of heteroclinic cycles in coupled cell systems with dihedral symmetry. In that work, the authors used the isotropy lattice of subgroups of the dihedral group as a mechanism to study the existence of heteroclinic cycles. An advantage of this mechanism over the more common analysis of stable and/or unstable manifolds is the fact that the isotropy lattice provides a systematic method for studying cyclic connections involving not only saddle nodes but also periodic solutions, resulting in a wide variety of cycles.

Next we proceed to identify a two-parameter region on the (c_{xy},c_{yx}) plane where stable multifrequency patterns such as $P(t)$ can exist, thus we now allow c_{yx} to vary. As c_{yx} changes, we observe relative small changes in the one-parameter bifurcation diagrams of Fig. 5 (results not shown here); the c_{xy} coordinate of each saddle-node point remains the same but the period T of the limit cycle at SN1 changes as c_{yx} varies. So we treat the period T as an additional bifurcation parameter. The top panel of Fig. 6 then shows the two-parameter continuation of SN1 for three different fixed values of T. Holding T fixed allows us to trace exactly the same limit cycle solution located at SN1. In the bottom panel of Fig. 6 we trace the locus of the stable multifrequency

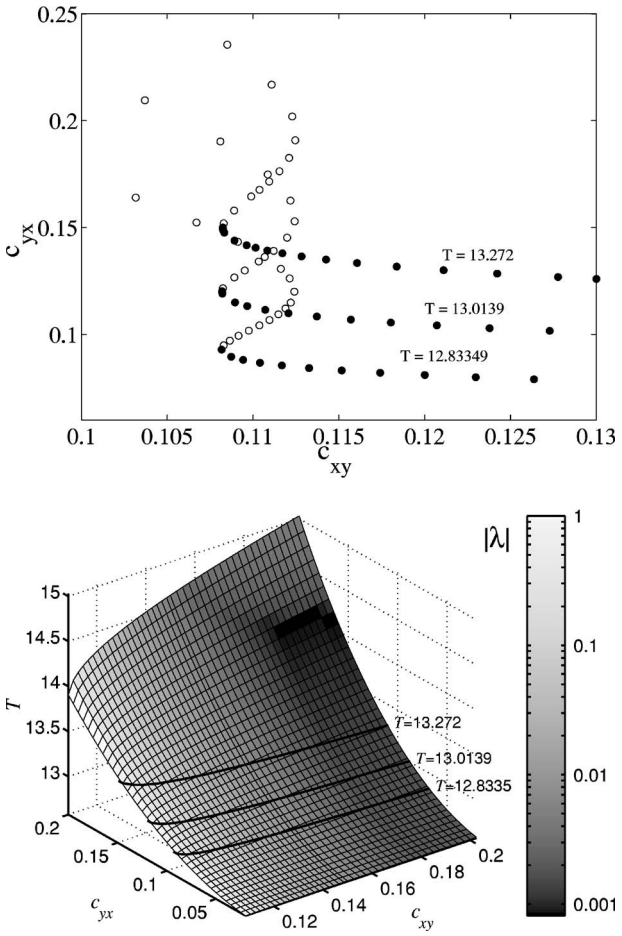

FIG. 6. Top, two-parameter continuation of the bifurcation diagram shown in Fig. 5. Filled and/or empty circles indicate stable and/or unstable periodic solutions, respectively. Bottom, stable multifrequency branch in the three parameter space (c_{xy}, c_{yx}, T). The shading corresponds to the modulus of the first nontrivial eigenvalue μ of the multifrequency pattern (darker corresponding to more stable, please note the logarithmic scale in the shading). As a guide, the three stable branches of the top panel are included (thick black lines). Since linear stability was computed using a time map from t to $t+T$, the stability eigenvalues μ_j are associated with a discrete map and thus the stability condition is $|\mu_j|<1$.

pattern in the three-parameter space (c_{xy}, c_{yx}, T). The shading of the locus corresponds to the modulus of the largest nontrivial eigenvalue μ (there is always a trivial eigenvalue $|\mu_k|=1$ in a direction tangent to the cycle). As one can expect, $|\mu|$ approaches one when c_{xy} approaches c_{xy}^{sn1} where the multifrequency cycle disappears in the above-mentioned saddle-node bifurcation. It is also interesting to note that the dark shaded area on the top right part of the locus $[(c_{xy}, c_{yx}, T) \approx (0.19, 0.16, 14.2)]$ corresponds to the region with most stable limit cycles. As the unstable limit cycles are concerned, the top empty circle in the top panel of Fig. 6 corresponds to a multifrequency cycle with an eigenvalue of $|\mu| \approx 71$ (this value rapidly increases to several thousands as c_{yx} is increased further). The large magnitude of this eigenvalue indicates that the cycles that are in the unstable region develop their instability in a very short period of time and, thus, are not experimentally viable.

The continuation of the SN2 point yields loci curves similar to those shown in Fig. 6. The same conclusion applies to SN3 and SN4, except that the loci curves are now located in the second quadrant, $(c_{xy}<0, c_{yx}>0)$, a direct result of the reflectional symmetry seen in the one-parameter bifurcation diagram of T against c_{xy}, see bottom panel in Fig. 5. The following observations apply to the continuation diagrams shown in Fig. 6. The loci of SN1 never cross the axes of the parameter plane (c_{xy}, c_{yx}). Also, stable multifrequency patterns only exist in the open region $c_{xy}>c_{xy}^{\mathrm{sn1}}=0.1082$, indicating the natural restriction that the coupling TW $\rightarrow$ IP must be strong enough to support the multifrequency pattern. However, more importantly, if a desired frequency for the pattern must be achieved, then, for small c_{yx}, c_{xy} must increase to make up for the lack of interplay dynamics. In this region $(c_{xy} \gg 1)$, however, the interplay between the two arrays closely resembles the interaction of a master-slave interaction. Nonetheless, for practical applications of actual coupled oscillator devices, the mutual coupling between units is typically small. It is clear that one could devise a coupling scheme that uses a series of amplifiers in order to increase the coupling strength. However, such a device would definitely have some, potentially serious, disadvantages, (a) device more difficult and expensive to build, (b) device more expensive to operate (more power needed), (c) real oscillators are likely to saturate for high input power, and (d) device much bulkier and thus reducing the range of potential applications. Therefore, for experimentally feasible and practical parameter values, it is more desirable that the multifrequency pattern emerges from the mutual interaction of the arrays rather than from a master-slave interaction. In order to strengthen this argument we present in Fig. 7 the dependence of the amplitude of the Y array as a function of the coupling parameters. This amplitude is defined by $A_y=\max\{\mathrm{Re}[y(t)]\}-\min\{\mathrm{Re}[y(t)]\}$ computed over the limit cycle. The top panel represents the typical behavior of A_y as the parameter c_{xy} increases from the saddle node c_{xy}^{sn1}. It is clear that as the coupling decreases so does the response of the Y array. However, the signal that the Y array receives is proportional to the coupling strength c_{xy}, and thus a better indicator on the efficiency of the multifrequency output is defined as the normalized amplitude A_y/c_{xy}. This normalized amplitude represents the conversion rate of the TW into the IP pattern, and thus it is an indicator of the efficiency of the multifrequency pattern. In the middle panel of Fig. 7 we depict this normalized amplitude for $c_{yx}=0.15$, where it is clear that a maximum conversion rate is achieved for $c_{xy}=c_{xy}^{M} \approx 0.1378$. This indicates that the best multifrequency conversion rate is attained at a relatively small value of c_{xy}. In fact, for other values of c_{yx}, $0.05 \leqslant c_{yx} \leqslant 0.25$, see bottom panel of Fig. 7, the local maximum conversion rate is located near the values of c_{xy} that are of the same order of magnitude as c_{yx}. This fact further supports the claim that the most efficient and practical multifrequency pattern is achieved when there is a truly mutual interaction between the arrays (i.e., when c_{xy} and c_{yx} are of the same order of magnitude). Nonetheless, it is interesting to note that for larger values of c_{yx} ($c_{yx}>0.2$ in Fig. 7), a larger conversion rate might be achieved with large values of c_{xy} ($c_{xy}>10$), even though

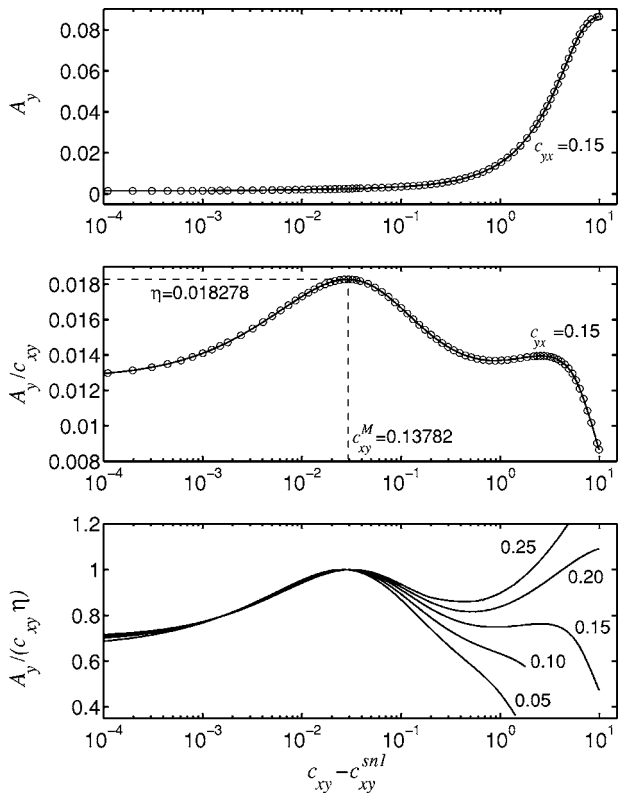

FIG. 7. Amplitude of the multifrequency oscillation as a function of the coupling parameters. Top, amplitude of oscillation for the Y array, A_y, as a function of the coupling parameter detuning $c_{xy}-c_{xy}^{\mathrm{sn1}}$ for $c_{yx}=0.15$. Middle, same as above but with the amplitude normalized by its input coupling. This normalized amplitude gives a direct measure of the amplitude of the multifrequency oscillations with respect to the coupling strength. Namely, it measures the conversion from TW to IP or, in other words, the multifrequency conversion efficiency. Bottom, same as middle panel for different values of c_{yx}. For a better comparison, each curve has been rescaled by η corresponding to the maximum depicted in the middle panel. For $c_{yx}=0.05$, 0.10, 0.15, 0.20, 0.25 the maximum normalized amplitudes are approximately $\eta=6.78\times10^{-4}, 5.41\times10^{-3}, 1.83\times10^{-2}, 4.33\times10^{-2}, 8.48\times10^{-2}$.

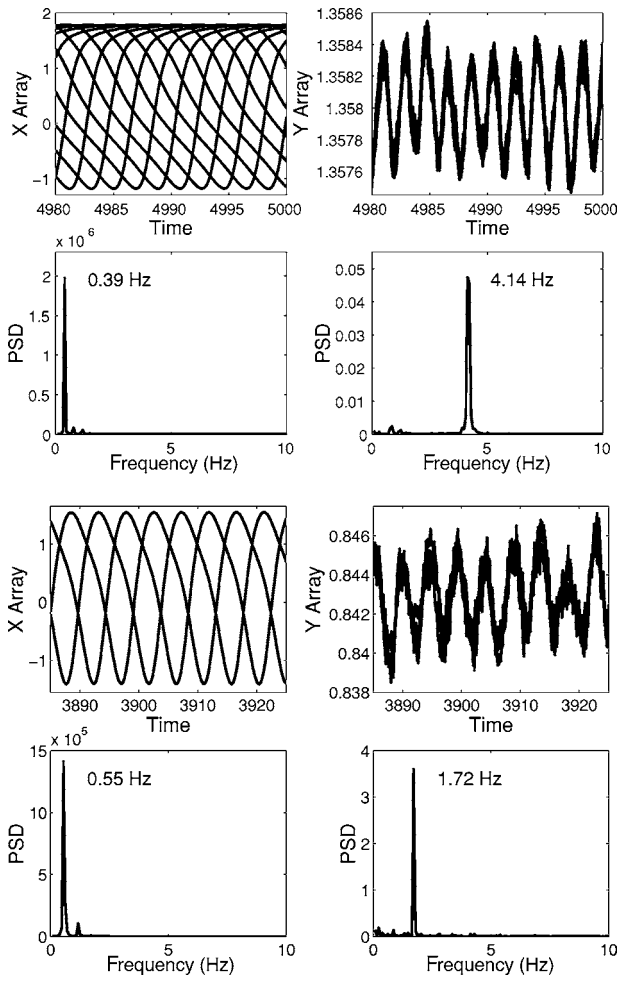

FIG. 8. Multifrequency oscillations under the presence of noise for $N=11$ (top four panels) and $N=3$ (bottom four panels) oscillators per array. Random, time dependent, noise has been added to the internal parameters of the oscillators. Each oscillator is perturbed independently with an external noise of 5% in ω_x and α_x and 0.5% in ω_y and α_y for $N=11$ (top panels) and 10% in ω_x and α_x and 5% in ω_y and α_y for $N=3$ (bottom panels). The unperturbed parameter values are $\alpha_x=\alpha_y=1.0$, $\omega_x=\omega_y=0.5$, $c_x=-0.4$, $c_y=0.4$, and $c_{xy}=c_{yx}=0.11$ for $N=11$; and $c_{xy}=0.19$ and $c_{yx}=0.16$ for $N=3$. Note that the parameter values for $N=3$ lie in the region with most stability depicted by the dark shaded area in Fig. 6.

there is a local maximum for the conversion rate around $c_{xy}\approx0.15$. This regime $(c_{xy}/c_{yx}\gtrsim50)$, which could be viewed as a master-slave regime, corresponds to coupling parameter values that are likely to saturate the Van der Pol oscillators and force them to work outside of practical operational ranges.

For practical applications of the proposed multifrequency mechanism it is important to study the robustness of the obtained multifrequency solutions. For this purpose let us introduce an external noise that breaks the homogeneity of the arrays. Since in the experimental applications it is straightforward to tune the coupling parameters (the different cells are usually coupled through tunable amplifiers), we focus our robustness analysis to nonhomogeneities at the level of the oscillator themselves. Let us then introduce an additive random perturbation to the internal parameters of the oscillators $(\alpha_x, \alpha_y, \omega_x, \omega_y)$. The perturbation is applied independently to each oscillator in both arrays by adding a random variable in $[0, 1]$ with a weight proportional to the unperturbed parameter. We typically used a 5%–10% perturbation in the X-array parameters (α_x, ω_x) and a 0.5%–5% perturbation in Y-array parameters (α_y, ω_y). The ensuing perturbed solution was found to contain a noisy component most visible in the multifrequency array Y. We have verified that other types of noise (cf. Gaussian) and a wide range of oscillator array sizes (from $N=3$ to $N=19$) did not qualitatively changed the results. As an example we depict in Fig. 8 typical multifrequency noisy patterns induced by a time dependent random noise in the oscillator parameters for $N=11$ (top four panels) and $N=3$ (bottom four panels) oscillators per array. As shown in Fig. 8, the oscillations in the Y array contain a noisy component on a multifrequency pattern. The X array also contains noise but it is not

very visible due to the spatial scale of the amplitude of the oscillations. Zooming in, however, would reveal the effects of noise on the amplitude of the wave. The power spectra density for the two arrays confirms that the multifrequency patterns with a ratio $N:1$ is preserved. Although the PSD spectrum of the oscillations in the heterogeneous network are not as clean as those of the homogeneous network, see Fig. 3 and Fig. 4, the PSD spectrum suggests a nominal frequency in the in-wave oscillations with small noise modulating the amplitude of the wave. It is also interesting to note that for $N=3$, the noise level that could be introduced to the system before destroying the multifrequency oscillations is quite large, 10% noise in X and 5% in Y. This is due to the fact that we chose parameter values where the multifrequency oscillations are the most stable. These parameters correspond to the dark shaded area in Fig. 6 around $(c_{xy}, c_{yx}) \approx (0.19, 0.16)$. This naturally suggests that in practical applications, where external noise is inherent, one should optimally choose the parameter values for a particular configuration to lie within the most stable parameter regions.

V. CONCLUSIONS

We have produced multifrequency patterns through two interconnected arrays of Van der Pol oscillators (each array consists of an odd number N of oscillators). The "fast," Y-array oscillates in-phase at a frequency N times faster than the "slow," X array, which generates a traveling wave pattern. Both patterns, IP and TW, are controlled via the cross couplings between the two arrays, c_{xy} couples TW$\rightarrow$IP and c_{yx} couples IP$\rightarrow$TW. Furthermore, we have found an open region in coupling parameter space $(c_{xy}>0, c_{yx}>0)$ where a family of stable multifrequency patterns exist for $c_{xy}>c_{xy}^{\mathrm{sn1}}$. The entire family is parametrized by the couplings strengths and the period T of the TW solution. Interestingly, however, is the fact that for a given fixed period T, and small c_{yx}, the stable multifrequency patterns only exist for large values of c_{xy}, which corresponds to a region of parameter space where the arrays behave as a master-slave system. On the other hand, the maximum multifrequency conversion rate TW$\rightarrow$IP occurs when the values of the two cross couplings are of the same order of magnitude. That is, the maximum conversion rate is attained when both arrays truly interact with each other, as opposed to one being the master and one the slave. The existence of multifrequency patterns in arrays with arbitrary number of oscillators depends upon network connections that can support the coexistence of a TW pattern and an IP solution. In principle, an array with $\mathbb{S}_N$ symmetry should include both types of solutions for any N, though their stability properties would certainly change. More details can be obtained through the theory of symmetry-breaking Hopf bifurcations applied to networks with $\mathbb{Z}_N$ symmetry [24,26,28–30]. The network of Fig. 2, in particular, exhibits multifrequency phenomenon for larger arrays. Table I summarizes the set of parameter values where these patterns have been observed, from $N=3$ up to $N=19$. A complete bifurcation analysis of each individual case is beyond the scope of this work.

TABLE I. Parameter values for various cases of multifrequency patterns observed through simulations of the network equations (7).

$N=M$	k_x	α_x	ω_x	k_y	α_y	ω_y	$c_{xy}=c_{yx}$
3	−0.4	1.0	0.5	0.4	1.0	0.5	0.12
5	−0.5	1.0	0.5	0.5	1.0	0.5	0.12
7	−0.3	1.0	0.5	0.3	1.0	0.5	0.06
9	−0.3	1.0	0.5	0.3	1.0	0.5	0.06
11	−0.3	1.0	0.5	0.3	1.0	0.5	0.06
13	−0.3	1.0	0.5	0.3	1.0	0.5	0.03
15	−0.3	1.0	0.5	0.3	1.0	0.5	0.035
17	−0.4	1.0	0.5	0.4	1.0	0.5	0.035
19	−0.45	1.0	0.3	0.45	1.0	0.3	0.034

It would also be interesting to study what happens when the arrays do not have the same number of oscillators, but such change would lead to a different type of network, i.e., an interconnected system of different subnetworks, which cannot be considered as a small perturbation. For this reason we defer consideration of this case for future work. From an experimental point of view, a circuit implementation of the network model equations is limited by the choice of cross-coupling functions that can satisfy operational regimes (cf. avoid a saturation of the oscillators). Nevertheless, the evidence presented in this paper suggests that the most experimentally viable option for the sustainability of multifrequency rhythms derives from the mutual interaction between the arrays.

For practical applications it is important to study the effects generated by the fact that in practice the oscillators are not identical. Also, random, temporal, variations of the parameters could be induced by a noisy environment. In order to test the robustness of the multifrequency patterns to these imperfections, we added large levels of (time dependent) noise in the internal parameters for each individual oscillator independently. The results presented here demonstrate that, by choosing the unperturbed internal parameters of the oscillators to lie within appropriate stability regions, noise levels of 5%–10% can be absorbed by the array without destroying the multifrequency pattern. This noise level is well within expected levels induced in typical applications. The experimental setup of these ideas is currently in progress and will be reported in a future publication.

ACKNOWLEDGMENTS

Informative discussions with Luciano Buono and Marty Golubitsky are gratefully acknowledged. The authors acknowledge support from the Office of Naval Research (Code 331). Two of the authors (P.L. and A.P.) were supported in part by a grant from the San Diego Foundation Blasker-Rose-Miah Fund C-2003-00307. One of the authors (R.C.G.) would like to acknowledge the support from the San Diego Foundation Grant-in-Aid program.

[1] D. G. Aronson, M. Golubitsky, and M. Krupa, Nonlinearity **4**, 861 (1991).
[2] E. J. Doedel, D. G. Aronson, and H. G. Othmer, IEEE Trans. Circuits Syst. **35**, 810 (1988).
[3] P. Hadley, M. R. Beasley, and K. Wiesenfeld, Phys. Rev. B **38**, 8712 (1988).
[4] P.-L. Buono, M. Golubitsky, and A. Palacios, Physica D **143**, 74 (2000).
[5] *Neural Control of Rhythmic Movements in Vertebrates*, edited by A. Cohen, S. Rossignol, and S. Grillner (Wiley, New York, 1988).
[6] M. Golubitsky, I. N. Stewart, P.-L. Buono, and J. J. Collins, Physica D **115**, 56 (1998).
[7] N. Kopell and G. B. Ermentrout, Math. Biosci. **89**, 14 (1988).
[8] N. Kopell and G. B. Ermentrout, SIAM J. Appl. Math. **50**, 1014 (1990).
[9] R. H. Rand, A. H. Cohen, and P. J. Holmes, in *Neural Control of Rhythmic Movements in Vertebrates*, edited by A. H. Cohen, S. Rossignol, and S. Grillner (Wiley, New York, 1988) pp. 333–367.
[10] X. Wang and J. Rinzel, Neural Comput. **4**, 84–97 (1992).
[11] W. J. Rappel, Phys. Rev. E **49**, 2750 (1994).
[12] K. Wiesenfeld, C. Bracikowski, G. James, and R. Roy, Phys. Rev. Lett. **65**, 1749 (1990).
[13] L. M. Pecora and T. L. Carroll, Phys. Rev. Lett. **64**, 821 (1990).
[14] C. W. Wu and L. O. Chua, Int. J. Bifurcation Chaos Appl. Sci. Eng. **4**, 979 (1994).
[15] R. M. May, Science **186**, 645 (1974).
[16] R. M. May, J. Theor. Biol. **51**, 511 (1975).
[17] R. M. May, Nature (London) **261**, 459 (1976).
[18] J. S. Halow, E. J. Boyle, C. S. Daw, and C. E. A. Finney (unpublished).
[19] G. B. Ermentrout and J. Rinzel, Am. J. Physiol. **246**, 102 (1984).
[20] J. Buck and E. Buck, Science **159**, 1319 (1968).
[21] T. Heath, K. Wiesenfeld, and R. A. York, Int. J. Bifurcation Chaos Appl. Sci. Eng. **10**, 2619 (2000).
[22] B. K. Meadows *et al.*, Proc. IEEE **90**, 882 (2002).
[23] D. Armbruster and P. Chossat, Phys. Lett. A **254**, 269 (1999).
[24] M. Golubitsky, M. Pivato, and I. Stewart Dyn. Syst. **19**(4), 389 (2004).
[25] M. Golubitsky and I. Stewart, in *Hopf Bifurcation with Dihedral Group Symmetry*, edited by M. Golubitsky and J. Guckenheimer, AMS Contemporary Mathematics 56 (Springer, New York, 1986), p. 131.
[26] M. Golubitsky and I. Stewart, in *Geometry, Mechanics, and Dynamics*, edited by P. Newton, P. Holmes, and A. Weinstein (Springer, New York, 2002), p. 243.
[27] A. Takamatsu, R. Tanaka, H. Yamada, T. Nakagaki, T. Fujii, and I. Endo, Phys. Rev. Lett. **87**, 078102 (2001).
[28] M. Golubitsky and I. N. Stewart (unpublished).
[29] M. Golubitsky and I. Stewart, in *Pattern Formation in Continuous and Coupled Systems*, edited by M. Golubitsky, D. Luss, and S. H. Strogatz, IMA Volumes in Mathematics and its Applications 115 (Springer, New York, 1999), pp. 65–82.
[30] M. Golubitsky, I. N. Stewart, and D. G. Schaeffer, *Singularities and Groups in Bifurcation Theory: Vol. II*, Appl. Math. Sci. 69 (Springer-Verlag, New York, 1988).
[31] R. Gambill and J. Hale, J. Rat. Mech. Anal. **5**, 353 (1956).
[32] R. Tiwari and R. Subramanian, J. Sound Vib. **47**, 501 (1976).
[33] V. In, A. Kho, J. D. Neff, A. Palacios, P. Longhini, and B. K. Meadows. Phys. Rev. Lett. **91**, 244101 (2003).
[34] B. Dionne, M. Golubitsky, and I. Stewart, Nonlinearity **9**, 559 (1996).
[35] B. Dionne, M. Golubitsky, and I. Stewart, Nonlinearity **9**, 575 (1996).
[36] E. Doedel and X. Wang, "Auto94: Software for continuation and bifurcation problems in ordinary differential equations," Applied Mathematics Report, California Institute of Technology, 1994.